Comparison of plasma performance and transport between tangential co- and counter-NBI heated MAST discharges

R.J.Akers 1), P.Helander 1), A.Field 1), C.Brickley 1), D.Muir 1), N.J.Conway 1), M.Wisse 2), A.Kirk 1), A.Patel 1), A.Thyagaraja 1), C.M.Roach 1) and the MAST and NBI teams.

1) EURATOM/UKAEA Fusion Association, Culham Science Centre, Abingdon, Oxon, OX143DB, UK.
2) Dept. of Physics, National University of Ireland , University College Cork, Cork, Ireland.

e-mail contact of main author: rob.akers@ukaea.org.uk

Abstract. High performance, counter Neutral-Beam Injection (NBI) heated plasmas have been produced for the first time in the Spherical Tokamak (ST), using MAST (I_p=1MA, n_e=5x10^{19}m^{-3}, R=0.9m, a=0.6m, κ=1.8) with ~3MW of neutral beams. Energy confinement time for ELMy H-mode reaches τ_E~150ms (approximately three times the level of quasi-steady-state, co-NBI heated H-mode, corresponding to H_H[IPB98(y,2)]~1.5 and plasma energy W~120kJ). A modest level of impurity accumulation (Z_{eff}~2-3, dominated by C^{6+}) is observed, resulting in "peaked" electron density profiles due to the increased neoclassical Ware pinch (in contrast to the "broad" profiles characteristic of co-NBI heated H-mode where Z_{eff}=1). Electron temperature profiles on the other hand become broad (again, in contrast to co-NBI where T_e is more peaked). Due to an increase in the applied torque (through the charge exchange loss of co-travelling, trapped fast ions) and possibly a reduction in momentum transport, toroidal rotation profiles become broad, with rotation velocities exceeding the plasma sound speed (V_φ~350km/s, Mach number M_φ~1). As a result, fuel density and Z_{eff} profiles cease to align with the temperature iso-surfaces, becoming skewed towards the low-field side consistent with theory. The dramatic increase in τ_E with counter-NBI (and corresponding broadening of T_e) correlates with a) a reduction in turbulent density fluctuations and b) the increase in toroidal rotation speed. Experimental data (supported by modelling), suggest that the improvement in energy and momentum confinement in counter-NBI heated discharges, is due to ExB flow shear suppression of micro-instabilities driven by the large, inherent, negative radial electric field (which for peak performance corresponds to a core radial potential of ~ -12kV).

1. Introduction

Auxiliary heating of the MAST spherical tokamak plasma is provided by two, tangentially orientated (tangency radius R_T=0.7m, primary energy E_0=40keV) Neutral Beam Injectors, typically delivering ~3MW of highly collimated, 40keV neutral deuterium beams. Fast ion orbits border on non-adiabaticity [1] due to the low magnetic field, requiring careful modelling of both the gyro- and guiding-centre orbital motion. Co-injection into MAST is well documented [2], model predictions agreeing with measured neutron rates, plasma energy, surface toroidal loop voltage and diamagnetic flux, indicating fast ion absorption efficiency close to 100% and plasma resistivity consistent with neoclassical theory. Peak performance for co-heating is typically achieved in H-mode (where confinement enhancement factor H_H[IPB98(y,2)] ranges from ~0.7 to ~1.1 depending upon Edge Localised Mode (ELM) frequency).

Due to the tendency for ELMs to deliver repetitive, damaging heat pulses to plasma facing components, together with their deleterious impact upon edge and core confinement, it is desirable to develop "ELM free" regimes with H_H>1. In this paper we describe a new high performance ST regime based around counter-NBI. ISX-B, ASDEX, and JFT-2M have all reported improved confinement using counter-NBI [3,4,5]. In addition, DIIID and AUG have studied counter- heated QH-mode plasmas [6,7] and DIIID is exploring the QDB scenario [8]. Clearly, such regimes do not lend themselves readily to "steady state", as NBCD acts against the plasma current. DIIID has, however, reported the observation of Edge Harmonic Oscillations (EHO) (the mechanism believed to be responsible for providing the cross-field particle transport in the QH/QDB mode pedestal) intermittently in co-injection heated

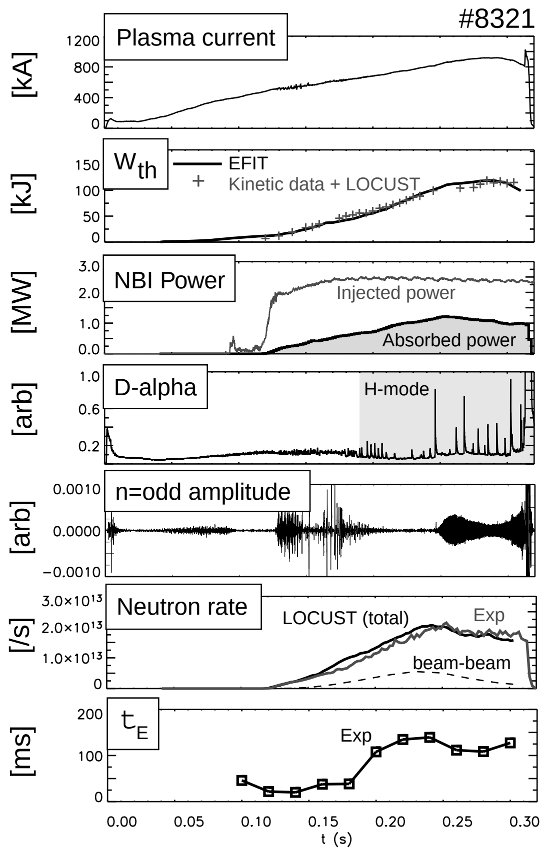

Fig. 1: Time traces for a typical, high performance counter-NBI heated H-mode plasma.

plasmas. By studying the micro-stability of such plasmas, together with the mechanism that eliminates the ELMs, it is thus hoped that steady state, high performance ELM-free alternatives may be found (for example using balanced beams [9,10]). Analysis is based around 12 counter-heated discharges and 11 co-heated plasmas for comparison. NBI modelling has been carried out using a combination of a) full gyro orbit simulations using the parallelised Monte Carlo code LOCUST [11] + EFIT (equilibrium fitting) and b) guiding centre simulations with Finite Larmor Radius correction using TRANSP/NUBEAM [12,13] and solution of the poloidal field diffusion equation.

2. Plasma energy and fast ion confinement

For the low current MAST plasmas used in this study (I_P~0.5-0.9MA), LOCUST and TRANSP indicate that only ~30-50% of the counter-injected fast ion power is absorbed by the plasma, due to trapped fast ions being born on the inner, rather than outer orbital leg [1]. Although deposited deep inside the plasma, many of the fast ions are promptly lost due to charge exchange in the molecular gas blanket surrounding the plasma (where n_{D2}~$10^{18}m^{-3}$) or through collisions with the internal poloidal field coils and protection armour. In contrast, the angular momentum delivered to the plasma is somewhat larger with counter- compared with co-NBI due to the rapid loss of predominantly co-moving NBI ions (thereby transferring angular momentum to the plasma through the resulting JxB torque [14]). Simulations predict an increase in applied torque of typically ~30-50%. Neutron rates (dominated by beam-thermal DD fusion) are significantly lower, as is power reaching the target Langmuir probes (reduced by a factor ~4 compared with co-NBI assuming $T_isep=T_esep$). It is notable therefore, that a number of counter-NBI heated MAST plasmas exhibit plasma energies comparable to the highest levels observed using co-NBI. Counter NBI ELMy H-mode is readily accessed (possibly due to the larger momentum injection modifying the edge radial electric field as suggested in [14]). Figure 1 shows time traces for a typical counter-NBI heated H-mode #8321. Plasma rotation, determined using charge exchange recombination spectroscopy (CXRS) for this discharge exceeds not only the carbon thermal velocity, but also the plasma sound speed (V_φ~00km/s at t=230ms, R=1.15m (slightly outboard of the magnetic axis), Mach number $M_\phi=\sqrt{2T_e/M_D}$ ~1.2). Magnetic fluctuation diagnostics indicate the presence of a significant fast ion population - high frequency activity (possibly compressional Alfvén modes [15] driven by the bump-on-tail in the fast ion distribution), appears at 130ms and subsides at 240ms. Plasma energy deduced from kinetic profile data and modelling for the fast ion content agrees very well with EFIT. The simulated neutron rate is also in good agreement with experiment, providing confidence in the >50% fast ion losses. τ_E (ignoring radiation losses) approaches ~50ms prior to L-H transition and the appearance of ELMs, increasing to ~150ms in the ELMy phase of the discharge, and reducing to ~100s with the onset of tearing mode activity. Figure 2 shows thermal energy confinement time τ_E versus the IPB98[y,2] scaling (where this time we have accounted for the radiated power in order to make a fair comparison between co- and counter-NBI discharges, due to radiation being a much larger fraction of the absorbed power for the latter). In the remainder of the paper, we have adhered to the ITPA convention. Co-NBI data are displayed as black and counter-NBI data as red points throughout. For counter-NBI, τ_E is typically up to ~2-3 times higher than for co-NBI discharges. Data then, are broadly consistent with reports from ASDEX [4] (where an increase in τ_E from ~ 43ms for co-injection to ~80ms for counter- is reported), and JFT-2M [5] where τ_E rose from 18ms for co- to 24ms during counter-NBI.

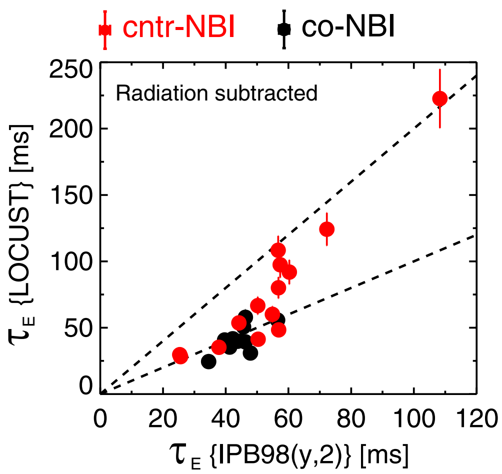

Fig.2: Thermal energy confinement time versus scaling IPB98[y,2]. Radiation has been subtracted due to the systematic difference between co- and counter-NBI.

3. Fuel and impurity particle transport

Another striking difference between co- and counter-NBI heated MAST discharges lies in the character of the electron density and temperature profiles. Figure 3 compares profiles for counter-NBI heated discharge #8322 and co-NBI heated H-mode discharge #8500. Co- heated discharges routinely exhibit broad density profiles (particularly in H-mode, often with edge density "ears" [16]) and "peaked" temperature profiles. Counter-NBI heated discharges on the other hand exhibit peaked density profiles and somewhat broader temperature profiles. Figure 4 shows a scatter plot of density peaking factor versus temperature peaking factor using 300pt Thomson scattering. ASDEX and JFT-2M both report a "peaking" of the density during counter-NBI heating (but not a broadening of the temperature profile). Similarly, QDB discharges exhibit a somewhat more peaked density [8] when compared with co-NBI heated discharges. For co-NBI heating on MAST, Z_{eff}, measured using 2D visible Bremsstrahlung imaging [17] is routinely flat and very close to 1.0. Figure 3e shows data for co-NBI heated discharge #8500. Counter-NBI heated discharges on the other hand are less pure (most likely due to sputtering of carbon from the upper divertor coil armour plate where the lost fast ion up-down asymmetric particle load is predicted to be of order ~2×10^{19} particles/s). Typically, Z_{eff} is ~2-3 and is peaked (see for example figure 3f),

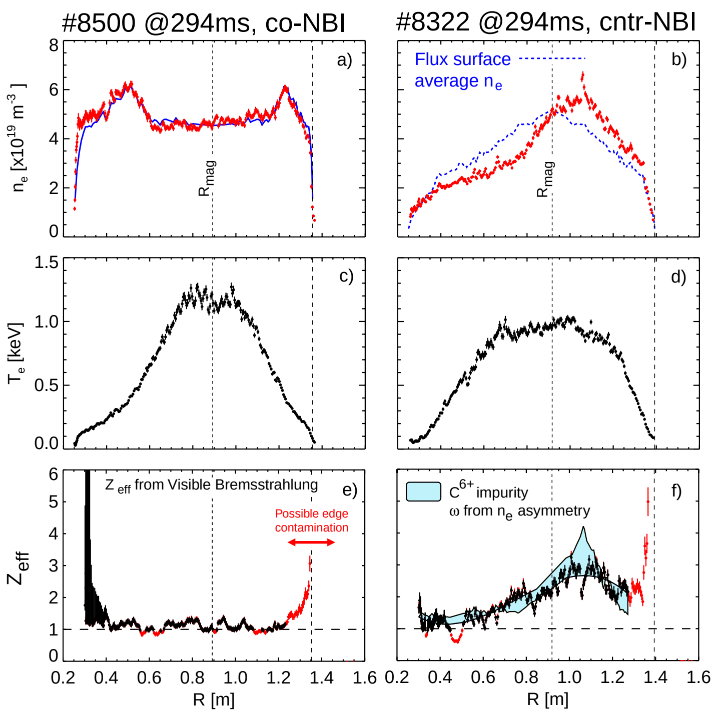

Fig.3: Electron density, temperature and Z_{eff} for co-NBI heated H-mode discharge #8500 and counter-NBI heated discharge #8322.

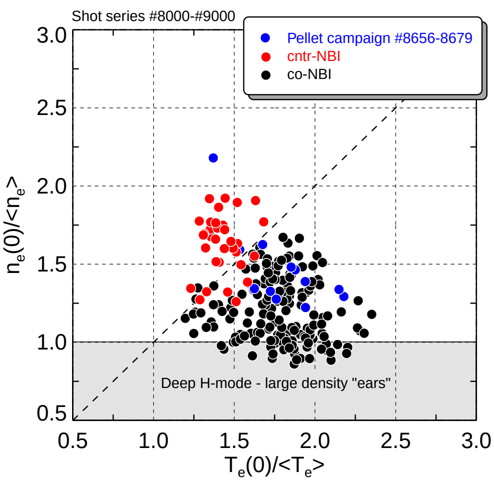

Fig.4: Electron density peaking factor versus temperature peaking factor for co- and counter-NBI heated discharges.

symptomatic of neoclassical impurity accumulation due to the peaked electron density [18]. The observed impurity concentration is, however, significantly less than values reported by DIIID for early QH mode development, being comparable to values achieved in AUG QH-mode following dedicated pre-shot boronisation [7]. Plasma impurity content is dominated by carbon (inferred from spectroscopy), similar to AUG (contaminated by C and O), but unlike DIIID (who report an elevated level of Ni). Such low values of Z_{eff}, achieved without the need for dedicated boronisation, are most likely due to the lack of close fitting plasma-facing components at the low field side. Poorly confined fast ions on MAST can orbit freely in the vacuum surrounding the plasma, reducing the level of carbon sputtering.

JFT-2M attribute the electron density peaking observed during counter-NBI to a drift-type micro-turbulence driven pinch [19], first introduced to explain the ISX-B results, which for JFT-2M proves reasonably consistent with the level and rate of observed peaking. The observation, however, that on all machines so far discussed, Z_{eff} is higher during counter-NBI suggests a simpler explanation. For the $T_e(0) \sim 1$ keV plasmas of ASDEX, JFT-2M and MAST, the increased Z_{eff} results in an enhanced Ware pinch [20], which is given in terms of the transport coefficients l_{11}^e and l_{13}^e by:

$$\left\langle \vec{\Gamma}_e \cdot \nabla\psi \right\rangle^{\rm pinch} = \frac{I}{m_e\tilde{\Omega}_0^2\tau_e}\left[\frac{\ell_\parallel^e Z_f}{Z_{eff}}\langle j_f B\rangle + \frac{1}{1+\nu_*}\frac{Z_f/Z_{eff}}{\langle B^{-2}\rangle}\left(\left\langle\frac{j_f}{B}\right\rangle - \left\langle\frac{1}{B^2}\right\rangle\langle j_f B\rangle\right) - \frac{\ell_{13}^2}{\langle B^2\rangle\langle B^{-2}\rangle}\frac{n_e e^2\tau_e}{m_e}\langle E_\parallel B\rangle\right]$$

The first and second terms comprise the NBCD driven pinch [21] (due to friction between the NBI ions and thermal electrons and essentially proportional to the unshielded beam driven current $<j_f B>$). The last part is the Ware pinch. Here, τ_e is the electron collision time normalised to Z_{eff}, B is the total magnetic field, $E_\parallel$ the local parallel radial electric field generated by the solenoid flux swing and $\Omega_0^2 = e^2/m_e<B^{-2}>$. For the discharges studied here, NBCD fraction is low – the 1st and 2nd terms can thus be neglected. Figure 5a shows the neoclassical pinch velocity determined using LOCUST/EFIT versus density peaking factor @r/a=0.9 for the co and counter-NBI heated discharges. Data are clearly anti-correlated (correlation coefficient ρ=-0.83) with the largest pinch velocity occurring for counter NBI (due to the

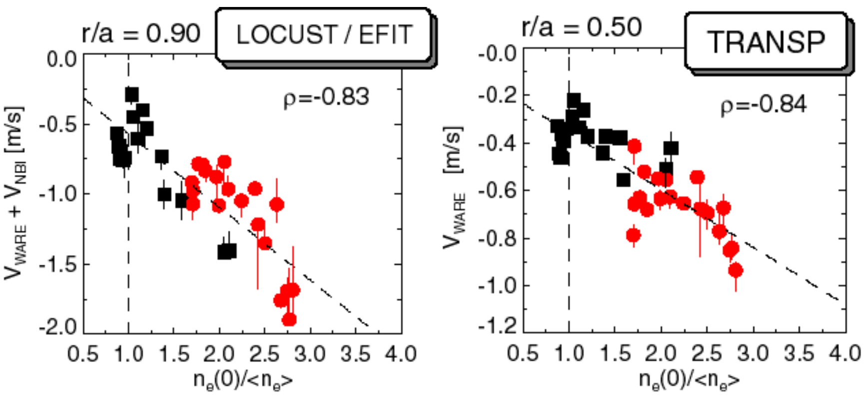

Fig.5: Pinch velocity versus electron density peaking factor at r/a=0.9 using LOCUST/EFIT and r/a=0.5 using TRANSP.

increased Z_{eff} driving a larger loop voltage). For core flux surfaces, $E_{\parallel}$ must be determined by evolving the poloidal field using TRANSP, resulting in the plot shown in figure 5b @r/a=0.5 (ρ=-0.84). At this radius, on average, the beam electron source exceeds the edge fuelling source (determined using mid-plane D_α array, TS data and target Langmuir probes with a 2-point scrape-off layer model), providing a reasonable level of confidence in the resulting level of particle diffusion. Due to unknown poloidal variation in gas fuelling flux, it is difficult to extract accurate values for individual discharges. Best estimates for the diffusion coefficients ($D<0.25m^2/s$), corresponding to radial velocities <1m/s are however consistent with the Ware pinch being strong enough to have a profound influence upon the density profile. Indeed, transport simulations for quasi-steady-state H-mode discharges indicate that core density evolution is completely dominated by beam fuelling and the neoclassical Ware pinch [22].

4. Plasma Rotation and momentum confinement

As has already been mentioned, plasma rotation during counter-NBI on MAST is large, exceeding levels so far observed during co-NBI, and as such can be measured using the in-out density profile asymmetry predicted in [23]:

$$n = n_0 \exp\left(\frac{m_i \omega^2 (R^2 - R_0^2)}{2(T_i + T_e)}\right) \quad \text{.............. (1)}$$

Figure 3b shows the measured and flux surface averaged density profile against major radius for #8322, indicating an "outward shift". The low aspect ratio of the ST (which provides a large difference in outer and inner flux surface radii), together with low moment of inertia, large applied torque (1-3Nm) and good momentum confinement (thus leading to large toroidal rotation speed ω) results in a clear in-out density asymmetry. Comparison with Charge Exchange Recombination Spectroscopy data over many discharges indicates a ~20% uncertainty for this technique [2]). Eqn. 1 can therefore be used to determine ω in the absence of CXRS rotation data. An additional asymmetry is also seen in the Z_{eff} profile data (figure 3f), adding another means by which plasma-rotation can be inferred. Mid-plane impurity density asymmetry is given by:

$$\frac{n_Z}{n_Z(0)} = \exp\left[\left(1 - \frac{T_e}{T_i + T_e} Z \frac{m_i}{m_Z}\right) \frac{m_Z \omega^2 (R^2 - R_0^2)}{2T_Z}\right] \quad \text{.............. (2)}$$

The large value of ω, and strong dependence upon impurity charge-state Z, thus provides a sensitive test of the bulk impurity species. The level of outward skew predicted by Eqn. 2, given rotation from Eqn. 1 (the shaded region in fig.3f), is consistent with the bulk impurity species being fully stripped carbon (supporting spectroscopy). Figure 6 shows plasma rotation frequency @r/a=0.5, measured using density asymmetry, against total applied torque using TRANSP for the co- and counter-NBI heated discharges. Plasma rotation rises sharply with increasing torque, with rotation profiles becoming broader as the applied torque is increased. On ASDEX, plasma momentum confinement is reported to have improved to a greater extent than energy confinement during counter-NBI [24] (although in [4], a clear increase in energy confinement was reported). There is some tentative evidence that in addition to increased rotation due to increased applied torque, momentum transport is likewise reduced on MAST (as one might

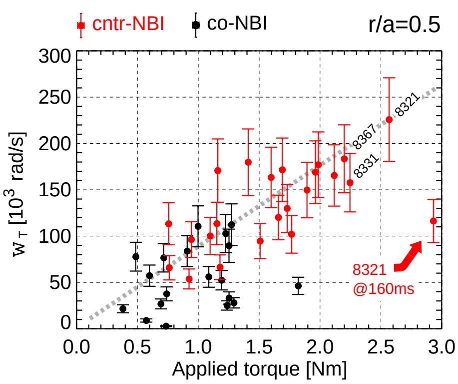

Fig.6: Plasma rotation frequency versus total applied torque from TRANSP.

expect due to the broader rotation profiles). χ_ϕ, determined using TRANSP and averaged between 0.3 and 0.6, drops from around ~0.6-2.0m^2/s to 0.3-1.0m^2/s.

5. Discussion and Summary

In [4], it is suggested that the improved level of counter-NBI confinement in ASDEX may be due to density peaking, as predicted by η_i theory [25]. In addition, theoretical work suggests that Trapped Electron Modes (TEMs) may be fully stabilised by collisions in the presence of a steep density gradient [26]. Many other tokamaks have indeed demonstrated improved confinement with peaked density profiles (see for example [27]), providing support for such theories. In contrast, however, JFT-2M [5] claim that their data are inconsistent with η_i theory predictions. Likewise, for MAST, although ion and electron temperature gradient (ITG/ETG) drive is absent ($\eta_i = \partial \ln T/\partial \ln n_e < 1$) in the core of counter-NBI heated discharges, $\nabla T_e \sim 0$ symptomatic of strong anomalous transport. Similar behavior is also seen near the axis of DIIID during QDB mode, as well as on other devices [8,28,29], but as yet, defies explanation. One possibility is that the core of MAST may be ergodised due to deleterious micro-tearing activity (as the flat magnetic shear, predicted by TRANSP for high performance counter-NBI discharges with a large I_P ramp (as in #8321 and #8322) is destabilising to micro-tearing [30]). Confinement is thus provided only in the outer part of the plasma.

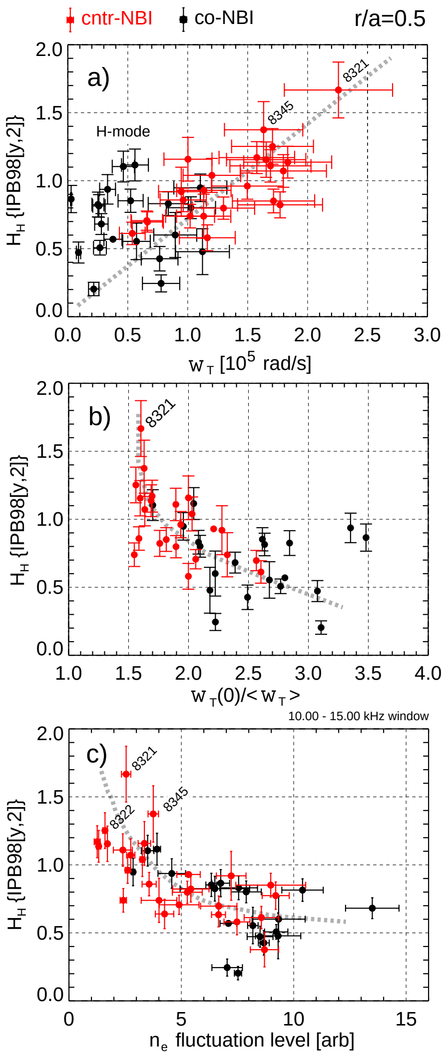

Fig.7: a) HH factor versus toroidal rotation frequency @r/a=0.5, b) HH versus rotation profile peaking factor and c) H_H versus density fluctuation level from interferometry.

Figure 7 shows H_H plotted against a) core rotation speed, b) rotation peaking factor and c) density fluctuation level determined by averaging the interferometer power spectrum between f=10 and 15kHz (taking care to avoid coherent tearing mode activity). Clearly, peak performance is achieved with a marked reduction in the level of fluctuations at the highest toroidal rotation velocities. Naively, one might expect the interferometer to be insensitive to density fluctuations due to the line-integrated nature of the measurement. JET, however, reports a similar observation prior to the onset of internal transport barriers [31]; in addition, CUTIE two-fluid electromagnetic turbulence simulations [32] produce similar fluctuation levels (corresponding to large, poloidally and toroidally rotating turbulent structures). It is well established that anomalous transport can be suppressed through the decorrelation of micro-turbulence by strong ExB flow shear [33], particularly in the presence of weak magnetic shear, (which reduces the instability growth rates [34], especially in the presence of large β' [35] due to a reduction of the drive due to curvature and ∇B drifts). Further, there is a suggestion that flow shear stabilisation may be somewhat easier at low aspect ratio due to the ratio of ExB shearing rate to instability growth rate scaling like $\omega_{SE}/\gamma_m \sim \rho_i^*$ [36]. The suppression of turbulence in the peripheral confinement zone of counter- heated plasmas may thus be explained by the large ExB shearing rates characteristic of counter-NBI heating. Indeed, this is the explanation proffered by DIIID to explain the prompt reduction in electrostatic modes, particularly at short wavelength seen during counter-NBI L-mode [37] (although without any observable increase in confinement). The high level of rotation on MAST, and broad profiles, together with the fact that the dominant $V_\phi B_\theta$ toroidal flow contribution to the radial electrostatic field E_r is augmented by the pressure gradient term, result in a large negative radial electrostatic field. Typically, the core plasma potential is ~-12kV, corresponding to a peak radial electric field of ~-400V/cm at r/a=0.35, larger in magnitude but similar in shape to data reported by JFT-2M. As a result, the radial electrostatic field creates a dramatic change in fast ion energy for "lossy" counter-pinch orbits as they traverse the full plasma minor radius. In contrast, for co-injection, the radial electric field peaks at r/a~0.3 with a magnitude typically +150V/cm (again, similar in shape to JFT-2M), passing through zero at r/a=0.75, slightly outboard of the JFT-2M radius of r/a=0.55. Figure 8 shows a) TS profiles, b) transport coefficients, c) current profile components and d) the ExB shearing rate for counter-NBI heated discharge #8302. This discharge exhibits one of the broadest electron temperature profiles so far observed on MAST due to a deliberate attempt to form an ITB, resulting in an extreme electron barrier. A detailed description of the experiment and the data is given in [38]. Reflectometry for this discharge indicates a reduction in turbulence in the barrier region (cut-off layer n_e~1.8×10^{19}m^{-3} @r/a~0.5). Similar observations are reported by DIIID during QDB mode where FIR measurements show a near complete suppression of long wavelength core turbulence (k~2cm^{-1}) with reflectometry indicating a reduction in the radial correlation length of the residual turbulence by as much as a factor 8 from L-mode [8]. Due to off axis peaking of the ohmic current density, augmented by the core counter- NBCD, the q-profile for #8302 has flat shear out to the foot of the ITB at r/a~0.5. GS2 gyrokinetic simulations [30] for a typical MAST flux surface (albeit in a different discharge #6252 with positive magnetic shear), yield ETG growth rates of order ~10^5-10^6s^{-1}. We note, therefore that the ExB shearing rate seen in #8302 (ω_{SE} ~ 10^6s^{-1}, approximately double that seen for co-NBI and also peaking at larger radius), approaches the "typical" level required to stabilise ETG modes on MAST (especially if ETG growth rates reduce at lower shear, as anticipated). It is also worth noting that although the ExB shearing rate exceeds the ITG growth rate, no ITB or clear broadening of T_i is evident in the ion channel. Of course, "any mechanism" which reduces χ_φ will clearly increase plasma rotation. In order to fully assess, therefore, whether the broad temperature profiles resulting routinely from counter-NBI (for which #8302 is an extreme example) are caused by the large inherent ExB shearing (as suggested in [37]), further transport and micro-stability analysis is required.

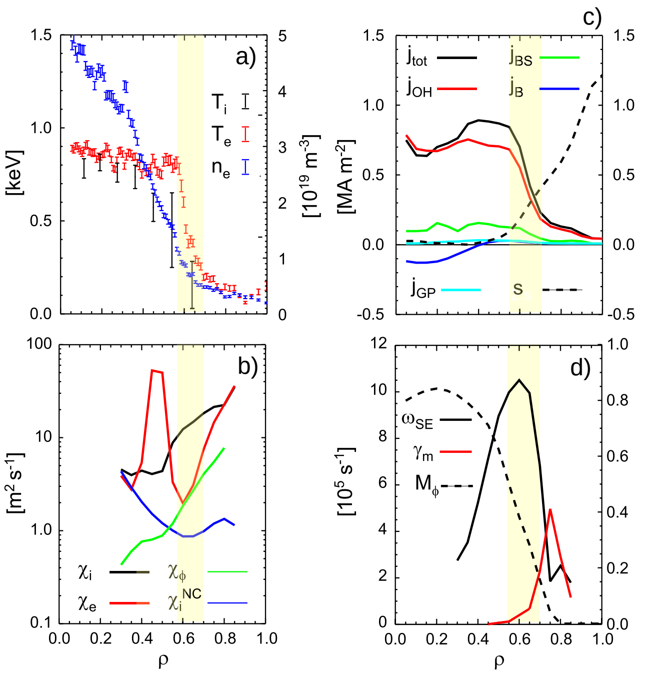

Fig.8: a) n_e and T_e profiles, b) transport coefficients, c) current components and d) rotation profile and ExB shearing rate.

To summarise, high performance counter-NBI heated discharges have been produced for the first time in the ST using up to 3MW of NBI. Although fast ion losses exceed 50%, plasma energies of order ~120kJ have been achieved (comparable with high performance co-NBI heated discharges), corresponding to τ_E typically ~2-3 times higher than for co-injection. Counter-NBI plasmas are characterised by a peaked Z_{eff} (with $Z_{eff}(0)$ typically ~2-3) and peaked electron density profiles resulting from the large neoclassical Ware pinch. Due to the increased torque, and possibly a reduction in momentum transport, plasma rotation can exceed the plasma sound speed, resulting in skewed electron density and Z_{eff} profiles consistent with theory. The increase in plasma confinement scales with toroidal rotation frequency and is accompanied by a reduction in density fluctuations. Experimental data (supported qualitatively by micro-stability calculations) suggest that the increased confinement is a result of ExB flow shear suppression due to the large, inherent negative radial electric field.

6. References

[1] D. Mikkelsen et al., Physics of Plasmas **4**, 10 3667 (1997).
[2] R. J. Akers et al., Plasma Phys. Control. Fusion **45**, A175 (2003).
[3] M. Murakami et al., in *Proc. of the 10th International Conference on Plasma Physics and Controlled Nuclear Fusion Research, London,* Vol. I, 87 (IAEA, Vienna) (1985)
[4] O. Gehre et al., Phys. Rev. Lett. **60**, 1502 (1988).
[5] K. Ida et al., Phys. Rev. Lett. **68**, 2 182 (1992).
[6] K. H. Burrell et al., Plasma Phys. Control. Fusion **44**, A253 (2002).
[7] W. Suttrop et al., Plasma Phys. Control. Fusion **46**, A151 (2004).
[8] C. M. Greenfield, Phys. Rev. Lett. **86**, 20 4544 (2001).
[9] E. J. Synakowski et al., Phys. Rev. Lett. **78**, 2972 (1997).
[10] H. Shirai et al., Nucl. Fusion **39**, 1713 (1999).
[11] R. J. Akers et al., Nucl. Fusion **42**, 122 (2002).
[12] R. J. Hawryluk, in Proc. of the Course in Physics Close to Thermonuclear Conditions, Varenna, (Commission of the European Communities, Brussels), Vol. I, 19 (1980).
[13] A. Pankin et al., Computer Physics Communications, **159**, 3, 157 (2004).
[14] J. Kim et al., Plasma Phys. Control. Fusion **38**, 1479 (1996).
[15] L. C. Appel et al., 31st EPS Conference on Plasma Physics, London, P4-195 (2004).
[16] R. Akers et al., Phys. Rev. Lett. **88**, 035002 (2002).
[17] A. Patel et al., *accepted for publication in* Rev. Sci. Instrum. **75**,11 (2004).
[18] M. R. Wade et al., Phys. Rev. Lett. **84**, 282 (2000).
[19] K. C. Shaing, Phys. Fluids **31**, 2249 (1988).
[20] A. A. Ware, Phys. Rev. Lett. **25**, 15 (1970).
[21] J.W. Connor and J.G. Cordey, Nucl. Fusion **14,** 185 (1974).
[22] M. Valovič, **EX/P6-30**, *this conference.*
[23] J. A. Wesson, Nucl. Fusion **37** 5, 577 (1997).
[24] A. Kallenbach et al., Plasma Phys. Control. Fusion **33** 6, 595 (1991).
[25] B. Coppi and C. Spight, Phys. Rev. Lett. **41**, 551 (1978).
[26] J. W. Connor and R. J. Hastie, Plasma Phys. Control. Fusion, **46**, 1501 (2004).
[27] B. J. D. Tubbing et al., Nucl. Fusion **31** 5, 839 (1991).
[28] B.W.Stallard et al., Phys. Plasmas **6**, 1978 (1998).
[29] M.Zarnstorff, Bull. Am. Phys. Soc. **43**, 1635 (1998).
[30] D. Applegate et al., *accepted for publication in* Physics of Plasmas, (2004).
[31] S. Sharapov et al., Phys. Rev. Lett. **93** 16, 165001 (2004).
[32] A. Thyagaraja, Eur. Journ. Mech. B Fluids, **23**, 475 (2004).
[33] T.S.Hahm, K.H.Burrell, Phys. Plasmas, **2** 5 1648 (1995).
[34] T.S.Hahm, Plasma Phys. Contr. Fusion., 44 A87 (2002).
[35] C.Bourdelle, Phys. Plasmas **10** 7 2881 (2003).
[36] M.Kotchenreuther, W.Dorland, Q.P.Liu et al., Nucl. Fusion, **40** 3Y 677 (2000).
[37] C. L. Rettig et al., Phys. Plasmas **3** 6, 2374 (1996).
[38] A. R. Field, **EX/P2-11**, *this conference.*

Acknowledgements. This work was jointly supported by the United Kingdom Engineering and Physical Sciences Research Council and EURATOM.